JVI Journals.ASM.org

Inactivation of the Human Cytomegalovirus *US20* Gene Hampers Productive Viral Replication in Endothelial Cells

Noemi Cavaletto, Anna Luganini, Giorgio Gribaudo

Department of Life Sciences and Systems Biology, University of Turin, Turin, Italy

ABSTRACT

The human cytomegalovirus (HCMV) *US12* gene family includes a group of 10 contiguous genes (*US12* to *US21*) encoding predicted seven-transmembrane-domain (7TMD) proteins that are nonessential for replication within cultured fibroblasts. Nevertheless, inactivation of some *US12* family members affects virus replication in other cell types; e.g., deletion of *US16* or *US18* abrogates virus growth in endothelial and epithelial cells or in human gingival tissue, respectively, suggesting a role for some US12 proteins in HCMV cell tropism. Here, we provide evidence that another member, *US20*, impacts the ability of a clinical strain of HCMV to replicate in endothelial cells. Through the use of recombinant HCMV encoding tagged versions of the US20 protein, we investigated the expression pattern, localization, and topology of the US20-encoded protein (pUS20). We show that pUS20 is expressed as a partially glycosylated 7TMD protein which accumulates late in infection in endoplasmic reticulum-derived peripheral structures localized outside the cytoplasmic virus assembly compartment (cVAC). US20-deficient mutants generated in the TR clinical strain of HCMV exhibited major growth defects in different types of endothelial cells, whereas they replicated normally in fibroblasts and epithelial cells. While the attachment and entry phases in endothelial cells were not significantly affected by the absence of US20 protein, US20-null viruses failed to replicate viral DNA and express representative E and L mRNAs and proteins. Taken together, these results indicate that US20 sustains the HCMV replication cycle at a stage subsequent to entry but prior to E gene expression and viral DNA synthesis in endothelial cells.

IMPORTANCE

Human cytomegalovirus (HCMV) is a major pathogen in newborns and immunocompromised individuals. A hallmark of HCMV pathogenesis is its ability to productively replicate in an exceptionally broad range of target cells, including endothelial cells, which represent a key target for viral dissemination and replication in the host, and to contribute to both viral persistence and associated inflammation and vascular diseases. Replication in endothelial cells depends on the activities of a set of viral proteins that regulate different stages of the HCMV replication cycle in an endothelial cell type-specific manner and thereby act as determinants of viral tropism. Here, we report the requirement of a HCMV protein as a postentry tropism factor in endothelial cells. The identification and characterization of HCMV endotheliotropism-regulating proteins will advance our understanding of the molecular mechanisms of HCMV-related pathogenesis and help lead to the design of new antiviral strategies able to exploit these functions.

Human cytomegalovirus (HCMV) is a ubiquitous opportunistic pathogen that persists throughout the lifetime of the infected host through both the chronic and latent states of infection. Generally, HCMV causes asymptomatic or mildly symptomatic infections in immunocompetent individuals. In contrast, primary infections or reactivations are a major cause of morbidity and mortality in immunocompromised hosts, such as transplant recipients and immunosuppressed and AIDS patients. HCMV is also the leading viral cause of congenital infections and birth defects in the developed world (1–4).

The 236-kbp genome of HCMV is the largest and most complex among those of the nine human herpesviruses (3, 5, 6). Even though its annotation remains provisional and its coding capacity has recently been proposed to be much greater than originally thought (7, 8), it is generally accepted that the HCMV genome encodes at least 170 canonical proteins (3, 5). Whole-genome functional profiling of two HCMV laboratory strains revealed that a set of only about 40 herpesvirus-common proteins, encoded by genes mainly located in the central region of the U_L domain, is required for productive viral replication in primary fibroblasts (5, 9, 10). The remaining two-thirds of canonical HCMV protein-coding genes, mostly betaherpevirus- or CMV-specific genes, are confined in the terminal regions of the genome (including the U_S domain) and are not essential in cultured fibroblasts. Although specific functions have yet to be assigned to many of these nonessential genes, they are mainly thought to be involved in regulating virus cell tropism, dissemination, and viral persistence within the host, as well as in the modulation of intrinsic, innate, and acquired host immune responses, thus contributing to viral pathogenesis in a variety of ways (3, 8). Within the U_S domain, a large group of nonessential genes cluster into families of related genes, each encoding 2 to 10 homologous open reading frames (ORFs) that can

Received 4 May 2015 **Accepted** 21 August 2015

Accepted manuscript posted online 26 August 2015

Citation Cavaletto N, Luganini A, Gribaudo G. 2015. Inactivation of the human cytomegalovirus *US20* gene hampers productive viral replication in endothelial cells. J Virol 89:11092–11106. doi:10.1128/JVI.01141-15.

Editor: K. Frueh

Address correspondence to Giorgio Gribaudo, giorgio.gribaudo@unito.it.

N.C. and A.L. contributed equally to this article.

occur either as tandem arrays (US2, US6, and US12 families) or in a dispersed manner within the U_S region or other parts of the HCMV genome (US1, US22, and G-protein-coupled-receptor [GPCR] families) (3, 6). The U_S gene families are involved in a variety of accessory functions (3, 5, 8). Indeed, members of the US2 and US6 families encode immunoevasion proteins that target various phases of the major histocompatibility complex class I (MHC-I) antigen-processing pathway, whereas the GPCR US27 and US28 genes encode potential seven-transmembrane (7TM)-spanning proteins: the US27 protein contributes to the efficient release of viral particles from infected cells, whereas the US28 gene products operate as chemokine receptors, stimulating cellular activation and migration (3, 5, 8). However, an unresolved issue in the functional characterization of the U_S region concerns the functions of the *US12* gene family that have yet to be assigned.

The *US12* gene family includes a set of 10 contiguous tandemly arranged genes (*US12* to *US21*) that are conserved only in HCMV and in CMVs specific to higher primates, such as those of the chimpanzee and of rhesus and cynomolgus macaques (7, 8, 11). The identification of putative hydrophobic seven-transmembrane domains (7TMD) in each of the *US12* ORFs would predict a common structural framework that associates these proteins with cellular membranes (11). In this regard, a low level of amino acid sequence similarity was observed between some *US12* family ORFs and the BAX Inhibitor-1 (BI-1) protein, which modulates apoptotic responses (11). Since deletion of individual *US12* family members or even the entire locus from the genome of HCMV laboratory strains was not found to affect viral replication in fibroblasts, these genes were thus classified as nonessential (9, 10). Consequently, it has been hypothesized that the *US12* genes may exert regulatory roles in the infection of specific cell types and/or under different physiological conditions *in vivo* (11); indeed, their conservation among clinical isolates sustains the idea of their importance and requirement during HCMV infection in the host (6, 12). Nonetheless, very little is known about the expression patterns and functions of individual US12 proteins in infected cells. In this regard, the intracellular localization of the US14, US16, US17, and US18 proteins was determined by immunofluorescence analyses that revealed an association with the cytoplasmic virion assembly compartment (cVAC), thus suggesting that their functions may be linked to virion maturation and egress (13, 14). In support of this hypothesis, it was observed that inactivation of the *US17* gene in producer fibroblasts results in increased production of noninfectious viral particles that can, in turn, deliver augmented amounts of the pp65 immunomodulatory tegument protein to newly infected cells, thus altering the regulation of both intrinsic and innate responses of cells infected with the US17-deficient virus (15). These data suggest a role of US17 in regulating adequate virion composition during HCMV maturation (15). Interestingly, two other US12 family members, US18 and US20, were recently shown to affect in fibroblasts the expression of the major histocompatibility complex class I (MHC-I) chain-related molecule (MICA), an NKG2D ligand induced by HCMV infection (16). Although the mechanism(s) of *US18*- and *US20*-mediated MICA downregulation remains to be established, these results suggest that *US18* and *US20* genes encode novel NK cell evasion factors that, by targeting MICA surface expression in the context of HCMV infection, contribute to the overall resistance of infected cells to NK cells (16).

Deletion of some *US12* genes has been reported to affect viral growth in cell types other than fibroblasts. Indeed, a major defective-growth phenotype was observed for a *US18*-null virus in cultured human gingival tissues (17), and we recently observed that deletion of US16 completely abrogated the replication of a clinical isolate in both epithelial and endothelial cells (ECs) (14). Interestingly, both *US16*- and *US18*-deficient viruses failed to express immediate-early (IE) genes in those cell types in which they were unable to replicate (14, 17), and pp65 and viral DNA did not move to the nucleus in endothelial and epithelial cells infected with a *US16*-null virus, thus suggesting defects during viral entry or in postentry events prior to IE gene expression, such as the transport of capsids to nuclei and release of viral genomes (14). At least in the case of genotypically *US16*-negative virions, the defective phenotype has since been related to a lack of adequate levels of the envelope glycoprotein complex required for efficient entry into endothelial and epithelial cells, which sustains the view that US16 exerts its function during the final stages of virus maturation (A. Luganini and G. Gribaudo, unpublished data).

In the present study, we characterized the protein expression and localization patterns of another *US12* family member, *US20*, and provide evidence that its inactivation abrogates viral replication in different types of endothelial cells without significantly affecting the ability of a clinical strain to productively replicate in both fibroblasts and epithelial cells. Although the adsorption and entry phases were not significantly altered in endothelial cells infected with a US20 mutant virus compared to cells infected with the wild-type (wt) virus, the expression of representative E and L mRNAs and proteins, as well as viral DNA synthesis, was severely impaired. These results suggest that the *US20* gene encodes a determinant of HCMV endotheliotropism that is required to sustain productive infection at a stage after entry but prior to the onset of E gene expression and viral DNA replication.

MATERIALS AND METHODS

Oligonucleotides. All oligonucleotides used for PCR, mutagenesis, and sequencing were obtained from Life Technologies. They are listed in Table 1.

Bioinformatics. US20 topology was predicted using algorithms SOSUI, TopPred 0.01, MEMSAT3, MEMSAT_SVM, and TMHMM 2.0. NetGlyc 1.0 was used to predict glycosylation sites, and ClustalW 1.8 was used to identify amino acid sequence alignments.

Cells and culture conditions. Low-passage-number primary human foreskin fibroblasts (HFFs; passages 12 to 18) were grown as monolayers in Dulbecco modified Eagle's medium (DMEM) (Biowest) supplemented with 10% fetal bovine serum (FBS) (Biowest), 2 mM glutamine, 1 mM sodium pyruvate, 100 U/ml penicillin, and 100 μg/ml streptomycin sulfate. Human dermal microvascular endothelial cells (HMVECs) (CC-2543) were obtained from Clonetics and cultured in endothelial growth medium (EGM) (Clonetics) as previously described (14). Human umbilical vein endothelial cells (HUVECs) were isolated by trypsin treatment of umbilical cord veins and cultured as HMVECs (14, 18). Lymphatic endothelial cells (LECs) were isolated and purified as previously described (18) and cultured on collagen type I-coated wells with EGM containing vascular endothelial growth factor-C (VEGF-C) (25 ng/ml). All experiments were performed using cells from the second to fifth passages for HUVECs and LECs and from the fourth to eighth passages for HMVECs. Retinal epithelial cell line ARPE-19 (ATCC CRL-2302) was cultured in a 1:1 mixture of DMEM (Biowest) and Ham's F12 medium (Life Technologies) supplemented with 10% fetal calf serum (FCS), 15 mM HEPES, 2 mM glutamine, 1 mM sodium pyruvate, 100 U/ml penicillin, and 100 μg/ml streptomycin sulfate.

TABLE 1 Oligonucleotides used for cloning, BAC mutagenesis, and PCR analysis

Primer designation	Sequence (5′ → 3′)[a]
US20-*galK*/*kan*-F	AGAGAAGGGTAGGTGCGCCGCAGCGGCTTTGTGCCGAGACCGTCGCCACCCCTGTTGACAATTAATCATCG
US20-*galK*/*kan*-R	CGCGGCTGCTGTGAAAATGAGCGCGGTTTTATAGGCATTAGGACTTCCCGCTCAGCAAAAGTTCGATTTA
US20-HA-F	AGAGAAGGGTAGGTGCGCCGCAGC
US20-HA-R1	CTAAGCGTAGTCTGGGACGTCGTATGGGTATCCTCCTCCCTGAAAATACAGGTTTTCTCCTCCGGACTTCCCGATCGTACTGG
US20-HA-R2	CGACAAGCGCGGCTGCTGTGAAAATGAGCGCGGTTTTATAGGCACTAAGCGTAGTCTGGGACGTC
US20-stop-F	AGAGAAGGGTAGGTGCGCCGCAGCGGCTTTGTGCCGAGACCGTCGCCACCATGCAGGCGCAGGAGGCTAACGCGCTGCT GC**tctaga**GCATGGAGGC
US20-stop-R	ACAAGCGCGGCTGCTGTGAA
US20-NV5-F1	GACCGTCGCCACCATGGGTAAGCCAATCCCTAACCCGCTCCTAGGTCTTGATTCTACGGGCGCCCAGGCGCAGGAGGCTA ACGC
US20-NV5-F2	AGAGAAGGGTAGGTGCGCCGCAGCGGCTTTGTGCCGAGACCGTCGCCACCATGGGTAAG
IE1 mRNA	
Forward	CACGACGTTCCTGCAGACTA
Reverse	TTTTCAGCATGTGCTCCTTG
UL44 mRNA	
Forward	GTGGAAACTGACGCGGTTAT
Reverse	ATCTAGATTTCGGCGTGGTG
UL99 mRNA	
Forward	GTGTCCCATTCCCGACTCG
Reverse	TTCACAACGTCCACCCACC
β-actin mRNA	
Forward	GTTGCTATCCAGGCTGTG
Reverse	TGTCCACGTCACACTTCA
IE1 forward	GACTAGTGTGATGCTGGCCAAG
IE1 reverse	GCTACAATAGCCTCTTCCTCATCTG
IE1 probe	AGCCTGAGGTTATCAGTGTAATGAAGCGCC

[a] Lowercase boldface letters indicate restriction enzyme sites.

Virus preparations and infections. The wild-type HCMV TR clinical strain was reconstituted by transfecting HFFs with the corresponding TR bacterial artificial chromosome (BAC) (a generous gift from Jay Nelson). The TR strain was derived from an ocular specimen (19) and cloned into a BAC (NCBI accession no. AC 146906) (12, 20).

TR mutants containing modifications in the *US20* gene (Fig. 1) were generated by a two-step replacement strategy using the *galK* recombineering method, as previously described (14, 21). In the first step, a *galK-kan* cassette was amplified from pGalK-Kan plasmid (a gift from D. Yu) by PCR using the US20-*galK*/*kan* primer set (Table 1) and then electroporated in *Escherichia coli* SW102 harboring the TR BAC. Several single kanamycin (Kan)- and Gal-positive TRΔUS20 colonies were further characterized for US20 replacement by PCR and sequencing and used to initiate the counterselection step. To generate TRUS20HA BAC, TRUS20stop BAC, and TRUS20NV5-CHA BAC (TRUS20NV5-CHA is a further variant of TRwt that expressed the US20 ORF with an HA epitope at the C terminus and a V5 epitope at the N terminus), the *galK-kan* cassette in TRΔUS20 BAC was replaced with the appropriate *US20*-modified gene cassette (generated with the primer sets shown in Table 1) as previously described (14). Gal-negative colonies were further selected for their inability to grow in the presence of Kan and then screened for the replacement of *galK-kan* sequences with modified versions of the US20 ORF by PCR, followed by restriction enzyme analysis and sequencing. Two independent TRΔUS20, TRUS20stop, TRUS20HA, and TRUS20NV5-CHA BAC clones were selected and characterized to ensure that their phenotypes did not result from an off-target mutation.

Infectious recombinant viruses (RV) TRΔUS20, TRUS20stop, TRUS20HA, TRUS20NV5-CHA, and TRwt were reconstituted in HFFs by cotransfection of the corresponding viral BAC and a plasmid expressing HCMV pp71 (a gift from T. Shenk) using SuperFect transfection reagent (Qiagen). Transfected HFFs were then cultured until a marked cytopathic effect was observed. Viral stocks and viral titers were obtained as previously described (14).

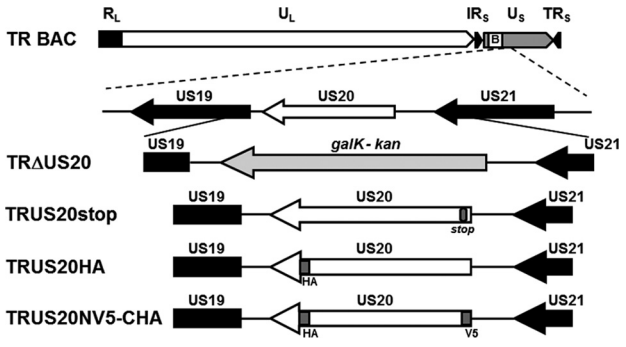

FIG 1 A schematic representation of the HCMV *US20* gene region and the modifications introduced into the US20 ORF. In TRΔUS20, the US20 ORF was replaced by a cassette containing the galactose kinase (*galK*) and the kanamycin resistance (*kan*) gene. In TRUS20stop, two nucleotide changes were introduced into codon 12, while a single nucleotide was changed in codon 13 of the US20 ORF to create a stop codon in the 12th codon, as well as a unique restriction site for XbaI. TRUS20HA was generated from TRΔUS20 by reintroducing the US20 ORF fused with the coding sequence for an HA epitope tag at its C terminus. TRUS20NV5-CHA was generated from TRΔUS20 by reintroducing the US20 ORF fused with the coding sequence for an HA epitope tag at its C terminus and a V5 epitope at the N terminus.

To determine the viral replication kinetics, HFFs, ARPE-19, or HMVECs were infected with TR BAC-derived viruses at a multiplicity of infection (MOI) of 0.01 PFU/cell for multistep growth analysis or an MOI of 3 for single-step growth analysis. Virus adsorptions were carried out for 2 h at 37°C. For all experiments, the time at which the virus was first added to the cells was considered time zero. At various times postinfection (p.i.), cells and supernatants were harvested and disrupted by sonication. Viral titers were then measured by an immediate-early antigen (IEA) (IE1 plus IE2) indirect immunoperoxidase staining procedure on HFF cells, as previously described (14).

For attachment and entry assays (see below), TRwt and TRUS20stop viral particles were concentrated from culture supernatants by centrifugation at 6,000 × *g* for 1 h at 4°C and then partially purified by passage through a 20% sorbitol cushion at 50,000 × *g* for 1 h at 4°C (14).

Immunofluorescence. Immunofluorescence analysis of viral antigens was performed as previously described (22–24) using rat monoclonal antibody (MAb) anti-hemagglutinin (anti-HA) (clone 3F10; Roche) and mouse MAbs against IEA (IE1 plus IE2) (clone E13; Argene Biosoft), UL44 (clone CH16; Virusys), UL99 (pp28) (clone CH19; Virusys), GM130 (clone 35/GM130; BD Biosciences), EEA1 (clone 14/EEA1; BD Biosciences), calreticulin (CALR) (clone 16/calreticulin; BD Biosciences), CD63 (sc-5275; Santa Cruz), gB (clone CH28; Virusys), and V5 (clone R960-25; Life Technologies). For selective permeabilization assays (25), cells were treated either with 20 μM digitonin (Sigma-Aldrich)–KHM buffer (110 mM potassium acetate, 20 mM HEPES, 2 mM $MgCl_2$) for 4 min at 4°C to selectively permeabilize the plasma membrane or with 0.1% Triton X-100–KHM buffer for 5 min to permeabilize all cellular membranes, as previously described (25). The binding of primary antibodies was detected with CF594-conjugated rabbit anti-mouse IgG antibodies (Sigma) or with CF488A-conjugated rabbit anti-rat IgG (Sigma). Nuclei were counterstained with DAPI (4′,6-diamidino-2-phenylindole) where indicated. Samples were then visualized with an Olympus IX50 fluorescence microscope equipped with Image-Pro Plus software. The intracellular localization of proteins was examined using an Olympus IX70 inverted laser scanning confocal microscope, and images were captured using FluoView 300 software (Olympus Biosystems).

Immunoblotting. Whole-cell protein extractions, determination of protein concentrations, and immunoblot analysis were performed as previously described (14). In certain cases, extracts were digested with endoglycosidase H (EndoH) (NEB), according to the manufacturer's instructions. Immunostaining was carried out with mouse MAbs against IEA (IE1 plus IE2), UL44, UL99 (pp28), and V5 or with rat anti-HA MAb conjugated to horseradish peroxidase (clone 3F10; Roche). Immunodetection of tubulin with a mouse MAb (clone TUB 2.1; Sigma) was used as a control for cellular protein loading. Immunocomplexes were detected with goat anti-mouse immunoglobulin antibodies conjugated to horseradish peroxidase (Life Technologies) and visualized by enhanced chemiluminescence (Western blotting Luminol reagent; Santa Cruz).

Quantification of immunoblot results was performed by densitometry using ImageJ software (version 1.46r; http://rsb.info.nih.gov/ij/docs/guide/146.html).

Attachment and entry assays. Attachment and entry assays in HMVECs were performed as previously described (26). In brief, to evaluate viral attachment, prechilled HMVEC monolayers were infected with equivalent amounts of precooled partially purified TRwt or TRUS20stop virions (normalized to equivalent genome copy numbers by real-time PCR). Cultures were centrifuged at 2,000 rpm for 15 min at 4°C and then incubated for 1 h at 4°C. After removal of the viral inocula, infected cells were washed twice with cold phosphate-buffered saline (PBS), harvested by scraping, pelleted by centrifugation, and stored at −80°C until assayed. As a control, separate infected cultures were washed twice with PBS at 4°C and immediately incubated with trypsin (100 μg/ml) for 15 min at 37°C (25). Protease inhibitor cocktail (Sigma P8340) (1×) was then added, and the cells were harvested, pelleted, washed, and stored at −80°C.

To evaluate viral entry, precooled partially purified TRwt or TRUS20stop virions were added to prechilled HMVECs and adsorbed for 1 h at 4°C as described above and then cells were washed twice with cold PBS, fed with fresh warm EGM, and incubated at 37°C. After 1, 2, or 4 h, cultures were washed twice with PBS and treated with trypsin as described above; cell pellets were then harvested and stored at −80°C. As a control, separate infected cultures were trypsinized immediately after adsorption at 4°C, washed twice with PBS, replated in fresh warm EGM, and incubated at 37°C for 5 h before harvesting of cell pellets was performed.

Quantitative viral nucleic acid analysis. Viral DNA was purified from RV stocks as previously described (14). To purify DNA from infected HMVECs, cell pellets were lysed in a digestion buffer containing proteinase K and the DNA was extracted twice using phenol-chloroform/isoamyl alcohol (25:24:1), and then was precipitated with ethanol (14). The number of viral DNA genomes per nanogram of cellular reference DNA (18S rRNA gene) was then assessed by real-time quantitative PCR (qPCR) using the previously described probe and primers to amplify a segment of the IE1 gene (Table 1) (14, 27, 28). Briefly, 50 ng of DNA from each sample was amplified in triplicate using Luminaris Color Probe Low ROX qPCR master mix (Thermo Scientific), containing the oligonucleotide primers and the TaqMan IE1 probe, dually labeled (5′, fluorescein 6-carboxyfluorescein [FAM]; 3′, 6-carboxytetramethylrhodamine [TAMRA] quencher) (27). After activation of Hot Start *Taq* DNA polymerase for 10 min at 95°C, samples underwent 45 cycles of 15 s at 95°C and 1 min at 60°C in an Mx 3000P real-time instrument (Stratagene) as previously described (14, 26). HCMV DNA copy numbers were normalized to the amount of human 18S rRNA gene (Assay-on-Demand 18S, assay no. HS99999901_s1; Applied Biosystems) amplified per reaction mixture. Standard curves were constructed using values from the serially diluted genomic cellular DNA from mock-infected HMVECs mixed with an IE1-encoding plasmid (29).

Real-time reverse transcription (RT)-PCR analysis was performed on an Mx 3000 P instrument (Stratagene) using SYBR green as a nonspecific PCR product fluorescent label. Total cellular RNA was extracted from infected cells using a NucleoSpin RNA kit (Macherey-Nagel) and retrotranscribed using a RevertAid RT kit (Life Technologies). cDNAs (or water, as a control) were then amplified in triplicate by real-time RT-PCR using SsoAdvanced Universal SYBR green Supermix (Bio-Rad) in a final volume of 20 μl. Primer sequences for assessing IE1, UL44, UL99 and β-actin mRNA levels are listed in Table 1. The optimized cycling conditions were as follows: polymerase activation and initial DNA denaturation at 95°C for 30 s, followed by 40 cycles of denaturation at 95°C for 15 s, primer annealing at 55°C for 1 min, and extension at 72°C for 1 min. For relative quantification analyses, semilogarithmic plots were constructed using delta fluorescence versus cycle number and a threshold was set for the changes in fluorescence at a point in the linear PCR amplification phase (threshold cycle [C_T]). The C_T values for each gene were normalized to the C_T values for the endogenous β-actin reference using the ΔC_T equation. The level of target RNA, normalized to the gene reference and relative to the level determined for the TRwt 12-h-infected cells (calibrator sample), was calculated by the comparative C_T method with the $2^{-\Delta\Delta CT}$ equation.

Statistical analysis. Data are expressed as the means and standard deviations (SD) of the results of independent experiments. Data were analyzed for significance using one-way analysis of variance (ANOVA) with the Bonferroni posttest correction for multiple comparisons. A P value of ≤ 0.05 was considered significant. All statistical tests were performed using GraphPad Prism version 5.01 for Windows (GraphPad Software).

RESULTS

Characterization of US20 protein expression. To characterize the expression and localization patterns of the protein encoded by the *US20* gene, we generated a derivative of the TR clinical isolate, termed TRUS20HA, expressing the US20 ORF as a fusion protein

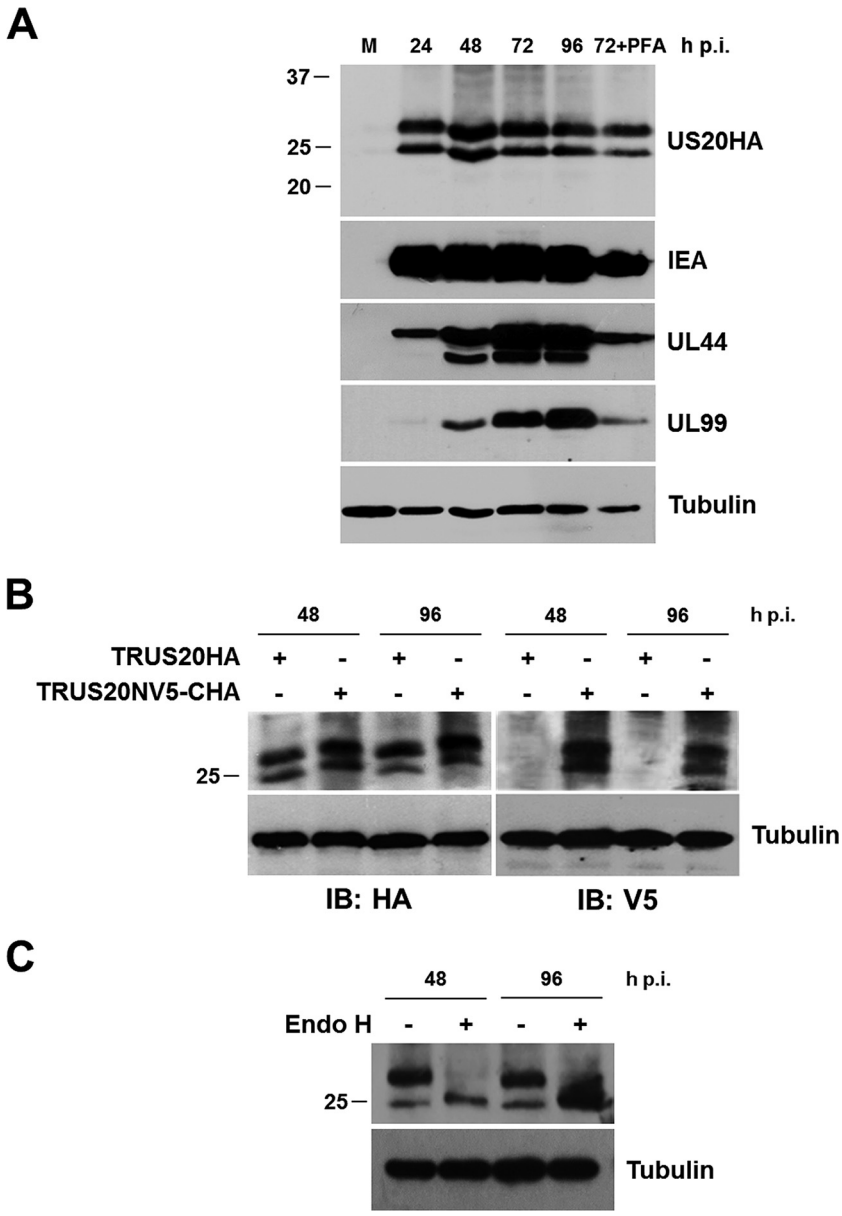

FIG 2 Expression of US20 protein. (A) Kinetics of pUS20HA expression during HCMV infection. HFFs were infected with TRUS20HA (MOI = 1 PFU/cell), and at the indicated times p.i., total protein cell extracts were prepared, fractionated by 12% SDS-PAGE (50 μg/lane), and analyzed by immunoblotting with anti-HA, IEA, UL44, UL99, or tubulin MAbs. The expression levels of IEA (IE1 and IE2 proteins could not be not resolved by means of the 12% SDS-PAGE used), UL44, and UL99 were assessed as controls for representative IE, E, and L HCMV proteins, respectively. The immunodetection of tubulin was performed as an internal control. Cell extracts were from mock-infected cells (M); cells infected for 24, 48, 72, and 96 h; or cells infected and treated with PFA (200 μg/ml) for 72 h. (B) The two US20HA protein bands share the same N terminus and C terminus. Protein extracts from HFFs infected with TRUS20HA or TRUS20NV5-CHA (MOI = 1 PFU/cell) were prepared at 48 and 96 h p.i., fractionated by 15% SDS-PAGE (50 μg/lane), and analyzed by immunoblotting (IB) with anti-HA, anti-V5, or tubulin MAbs. (C) EndoH treatment of pUS20HA. HFFs were infected with TRUS20HA (MOI = 1 PFU/cell), and at 48 and 96 h p.i., protein extracts were prepared. Aliquots (20 μg) were treated with EndoH (+) or incubated in buffer alone (−), fractionated by 12% SDS-PAGE, and then analyzed by immunoblotting with anti-HA or tubulin MAbs.

with an HA epitope at the C terminus (Fig. 1). Immunoblot analysis of the HA epitope of whole-cell protein extracts prepared at various time intervals from HFFs infected with TRUS20HA showed that US20 was expressed as a doublet of approximately 30 kDa and 25 kDa which could already be detected at 24 h p.i. (Fig. 2A). Accumulation of the pUS20HA doublet was insensitive to foscarnet (phosphonoformate [PFA]), which inhibits viral DNA replication, thus indicating that the *US20* gene is expressed with early (E) gene kinetics (Fig. 2A).

Since it has been reported that the US17 ORF is expressed in a segmented manner yielding two different polypeptides (30), we next investigated whether occurrence of the pUS20 doublet was the result of segmented expression of the full-length protein with a predicted size of 29.8 kDa. To verify this hypothesis, we gener-

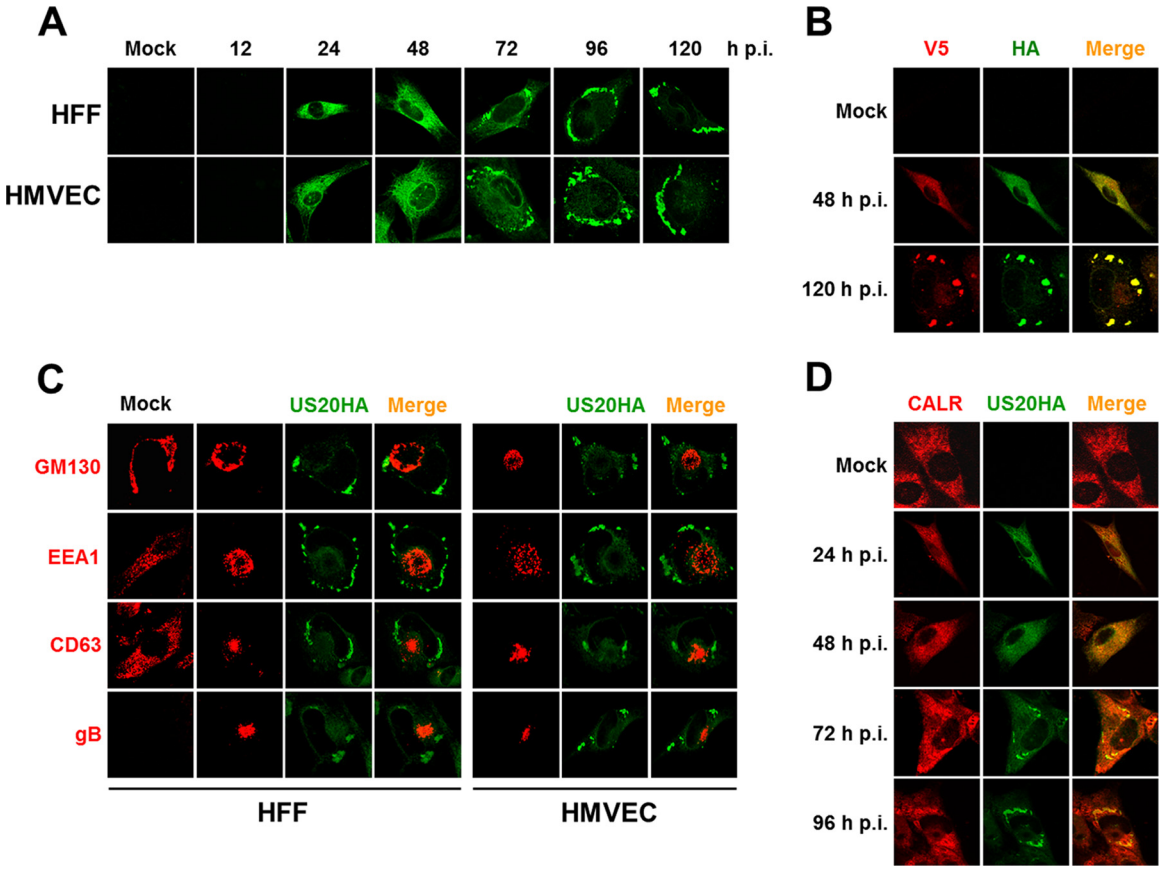

FIG 3 Intracellular localization of US20HA during HCMV infection. (A) Cytoplasmic localization of US20HA proteins in different cell types. HFFs or HMVECs were infected with TRUS20HA (MOI = 1 PFU/cell) or mock infected, and at various times p.i., cells were fixed, permeabilized, and immunostained with an anti-HA MAb. (B) The N and C termini of US20HA proteins colocalized during HCMV infection. HFFs were infected with TRUS20NV5-CHA (MOI = 1 PFU/cell) or mock infected, and at 48 and 120 h p.i., cells were fixed, permeabilized, and immunostained with anti-HA and anti-V5 MAbs. (C) US20HA accumulates late in infection outside the cVAC. HFFs or HMVECs were infected with TRUS20HA (MOI = 1 PFU/cell) or mock infected, and at 120 h p.i., cells were fixed, permeabilized, and stained for pUS20HA, GM130, EEA1, CD63, or gB. (D) pUS20HA localizes to ER membranes. HFFs were infected with TRUS20HA (MOI = 1 PFU/cell) or mock infected, and at various times p.i., cells were fixed, permeabilized, and immunostained for pUS20HA or calreticulin (CALR). The images shown in each panel (A to D) are representative of the results of three independent experiments.

ated TRUS20NV5-CHA, a further variant of TRwt that expressed the US20 ORF with an HA epitope at the C terminus and a V5 epitope at the N terminus (Fig. 1), which enabled simultaneous and independent detection of both ends of the full-length US20 protein. Immunoblot assays of extracts prepared from TRUS20NV5-CHA-infected HFFs revealed that the pUS20 doublet could be detected using anti-V5 or anti-HA MAbs (Fig. 2B). The molecular mass of the pUS20 doublet expressed by TRUS20NV5-CHA was slightly greater than that of the pUS20 detected by the use of anti-HA MAb in extracts from cells infected with TRUS20HA (Fig. 2B), thus confirming the successful addition of the V5 epitope tag at its N terminus. However, detection of the US20NV5-CHA doublet by both anti-V5 and anti-HA MAbs demonstrated that the faster-migrating pUS20s share terminal sequences at both ends with the slower migrating one, thus excluding segmented expression of the US20 ORF as a consequence of either usage of an internal alternative translational codon or proteolytic processing. This suggests that other posttranslational modifications, such as glycosylation, may contribute to generating the pUS20 doublet. To investigate this possibility, protein extracts were prepared from TRUS20HA-infected HFFs, treated with endoglycosidase H (EndoH), and then analyzed by immunoblotting. As shown in Fig. 2C, the doublet was converted by EndoH into a single band of about 25 kDa, thus demonstrating that the occurrence of two pUS20HA bands was due to different degrees of glycosylation and indicating that a fraction of pUS20 was not fully glycosylated.

The intracellular localization of pUS20HA at time points across the entire HCMV replication cycle in TRUS20HA-infected HFFs was then investigated by immunofluorescence analysis using the anti-HA MAb. According to the results of immunoblot analysis (Fig. 2A), anti-HA staining was first detectable at 24 h p.i. and displayed a diffuse pattern throughout the cytoplasm of infected cells up to 48 h p.i. (Fig. 3A). As infection progressed, starting from 72 h p.i., the intracellular localization of pUS20HA changed as it accumulated in distinct peripheral cellular cytoplasmic structures, which became increasingly evident at 96 h p.i.; by 120 h p.i., most of the pUS20HA was localized within these peripheral structures (Fig. 3A). This time-dependent pattern of pUS20HA cytoplasmic distribution was also observed in endothelial cells (HMVECs) infected with TRUS20HA (Fig. 3A). Moreover, the same intracellular localization of pUS20 was observed in

HFFs infected with the TRUS20NV5-CHA derivative, which, in addition to an HA epitope at the C terminus, expressed a V5 epitope at the N terminus of the US20 ORF (Fig. 3B). The extensive overlapping of the V5 and HA signals at both 48 and 120 h p.i. further supports the idea of the absence of any US20 segmentation as already observed by immunoblot analysis (Fig. 2B).

Next, we examined the intracellular localization of pUS20 relative to components of the cell secretory pathway that accumulate within the cytoplasmic virion assembly compartment (cVAC). The cVAC is a specialized compartment in HCMV-infected cells formed during the late stages of infection by modified and rearranged host organelles, including the Golgi apparatus, the trans-Golgi network, and endosomal structures. In the cVAC, HCMV virions undergo maturation where they acquire the final tegumentation and envelope before finally egressing from the cell (24, 31, 32). Since several US12 proteins, such as US14, US16, US17, and US18, have been observed to accumulate within the cVAC (13, 14), we investigated whether pUS20HA colocalized with any cellular or viral markers of cVAC. To this end, HFFs were infected with TRUS20HA and analyzed by immunofluorescence assay at 120 h p.i., a time when the cVAC was fully formed and the production of infectious virions was well under way. Nonetheless, as shown in Fig. 3C, we did not observe any significant colocalization of pUS20HA with GM130 (a *cis*-medial Golgi marker), EEA1 (an early endosomal marker), or CD63 (a late endosome marker) or with viral glycoprotein B (gB), which is known to accumulate in the cVAC. The displacement of pUS20HA from the cVAC was not cell type specific, since it was also observed in TRUS20HA-infected HMVECs (Fig. 3C). To define better the localization of pUS20 relative to other cellular membrane compartments, we investigated the potential association of pUS20HA with the endoplasmic reticulum (ER), which is known to be excluded from the cVAC formation site (24, 31, 32). To this end, the localization pattern of the ER marker calreticulin (CALR) was assessed in TRUS20HA-infected HFFs. As shown in Fig. 3D, at 24 and 48 h p.i., calreticulin displayed a typical diffuse staining pattern similar to that observed in mock-infected cells (Fig. 4A); however, by 72 h p.i., this pattern changed and calreticulin accumulated in structures that seemed to be completely displaced from the site where the cVAC was formed (Fig. 3D). Interestingly, calreticulin and pUS20HA signals almost completely overlapped at 24 and 48 h p.i., while the peripheral cytoplasmic structure to which pUS20HA accumulated became positive for calreticulin staining at late times of infection (Fig. 3D), thus indicating that pUS20 associated with ER-derived membranes over the entire replication cycle of HCMV. The same results were also obtained in HMVECs infected with TRUS20HA (data not shown).

Finally, to investigate the membrane topology of pUS20, we first predicted the potential transmembrane domain (TMD) regions using five different algorithms: SOSUI (33), TopPred 0.01 (34), TMHMM 2.0 (35), MEMSAT3, and MEMSAT_SVM (36). All algorithms were consistent in predicting a cytoplasmic N terminus and seven TMDs, thus indicating a predicted C terminus located on the luminal side of an internal membrane. To confirm this prediction and to determine whether the N- and C-terminal epitopes of pUS20NV5-CHA were cytosolic or luminal, an epitope accessibility assay was performed following selective permeabilization (25). To this end, HFFs were permeabilized either with 20 μM digitonin for 4 min, to permeabilize the plasma membrane only (while leaving internal membranes, such as the Golgi apparatus and the ER, intact), or with 0.1% Triton X-100 for 5 min, which allowed complete permeabilization and allowed antibodies to access epitope tags regardless of their orientation on the membrane (25). Protein markers of cell organelles, such as GM130 (a protein that is tightly bound to the cytosolic side of *cis*-Golgi membranes) (37) and calreticulin (a luminal ER protein) (38), were used to validate the selective permeabilization assay. Following digitonin treatment, GM130, but not calreticulin (CALR), was immunostained (Fig. 4A), thus validating these experimental conditions for the detection of membrane-associated epitopes with a cytosolic or luminal orientation. The orientation of both the N and C termini of pUS20 was therefore determined by immunostaining HFFs infected with TRUS20NV5-CHA with anti-V5 and anti-HA MAbs. Both digitonin treatment and Triton X-100 treatment enabled the anti-V5 MAb to access the N terminus of pUS20, with positive immunostaining results seen at both 48 and 96 h p.i. These results confirmed the cytosolic location of the N terminus of pUS20 as predicted by bioinformatics (Fig. 4B). In contrast, only complete cell permeabilization by Triton X-100 allowed immunostaining of the C-terminal HA tag of pUS20 (Fig. 4B), demonstrating that the C terminus of the protein was located on the ER lumen and thus confirming the predicted 7TMD topology of pUS20.

Taken together, the results shown in this section indicate that the early HCMV *US20* gene encodes a 7TMD protein that undergoes partial glycosylation and accumulates late in infection within cytoplasmic structures derived from the ER compartment and localized outside the cVAC.

HCMV US20-deficient viruses are defective for growth in endothelial cells. To investigate the requirement for US20 during the HCMV replication cycle in cell types known to be relevant for the virus's replication and dissemination in the host (39), we generated different US20-deficient viruses from the TR clinical isolate (19). Infectious viruses reconstituted from its BAC clone have been shown to productively replicate in endothelial and epithelial cells (20). In the derivative TRΔUS20, the entire US20 ORF was replaced with a *galK-kan* cassette (Fig. 1), whereas in the stop mutant termed TRUS20stop, the US20 coding sequence was changed in 3 bp to create a stop codon near the start of the ORF (Fig. 1). Infectious recombinant HCMVs were subsequently reconstituted in HFFs from two independently derived BAC clones for TRΔUS20 (clones 1.1 and 1.2) and TRUS20stop (clones 2.1 and 2.2) to reduce the chance of off-target mutations that might affect the observed cell growth phenotypes in a nonspecific manner. The growth exhibited by TRΔUS20 (clone 1.1) and TRUS20stop (clone 2.1) in fibroblasts under conditions of multistep or single-step growth was similar to the growth exhibited by TRwt and TRUS20HA (Fig. 5), thus confirming that expression of pUS20 is not required for productive replication in fibroblasts. The TRUS20HA derivative was included in all growth kinetics experiments as a control for a US20 revertant virus, since it was generated by replacing the *galK-kan* cassette of TRΔUS20 (clone 1.1) with the US20 coding sequence fused in frame with a C-terminal HA epitope (Fig. 1).

To determine the viral growth kinetics of US20-deficient viruses in other cell types, endothelial cells (HMVECs) and epithelial cells (ARPE-19) were infected with TRwt, TRΔUS20 (clone 1.1), TRUS20stop (clone 2.1), or TRUS20HA at an MOI of 0.01 for multistep growth analysis or at an MOI of 3 for single-step growth analysis and were titrated for detection of infectious virus

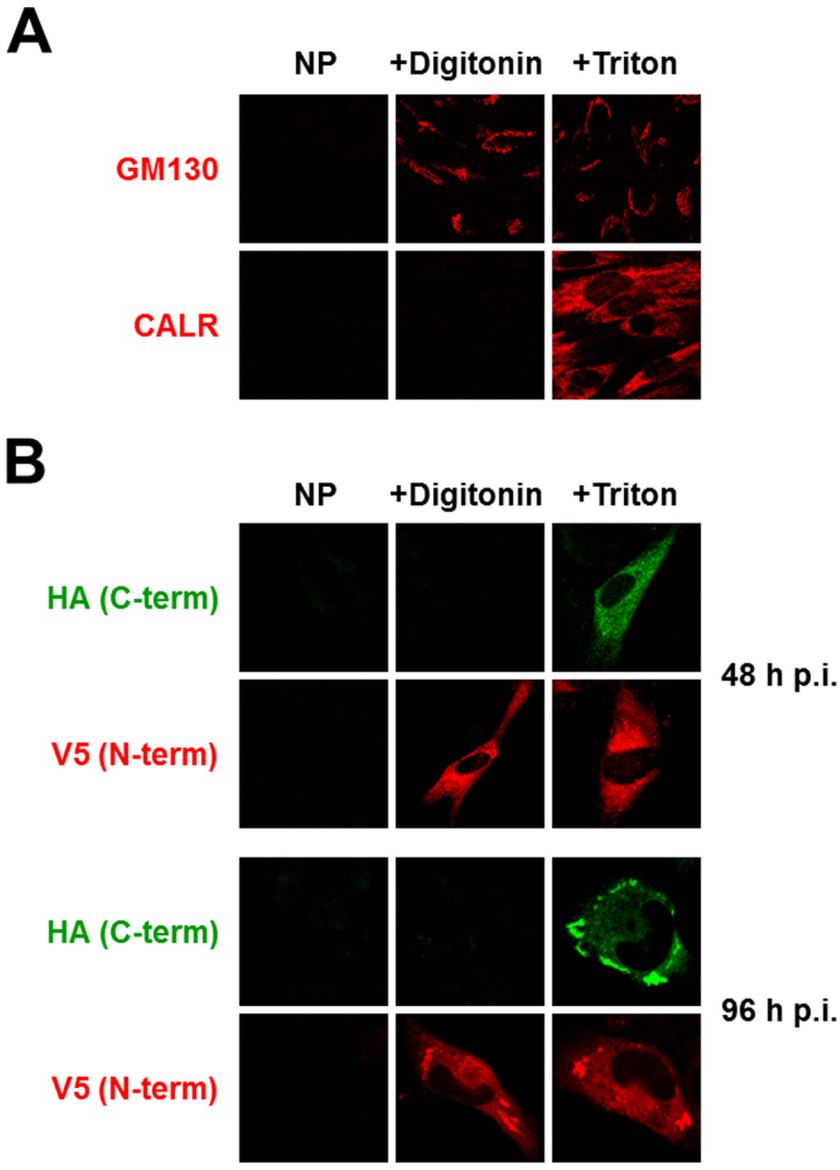

FIG 4 Membrane topology of pUS20. HFFs were infected with TRUS20NV5-CHA (MOI = 1 PFU/cell), and at 48 h or 96 h p.i., cells were selectively or completely permeabilized using digitonin (+Digitonin) or Triton X-100 (+Triton), respectively, or were not permeabilized (NP). The pUS20 N- and C-terminal tags were then immunostained with MAbs to V5 and HA, respectively (panel B). GM130 and calreticulin (CALR) staining of mock-infected cells was used to control for selective permeabilization (panel A). Data are representative of the results of three independent experiments.

at 0, 2, 4, 6, 8, 10, and 12 days p.i. The replication kinetics of the US20-deficient mutants in ARPE-19 cells at both MOIs were similar to those of the parental TRwt and the revertant TRUS20HA (Fig. 5). In contrast, under the multistep growth conditions, US20-null viruses exhibited a decrease of more than 4 log units in titer in HMVECs starting on day 8 and up to 12 days p.i. in comparison to TRwt (Fig. 5). The severe replication defect of TRΔUS20 and TRUS20stop viruses was observed even in single-step growth curves (Fig. 5), thus indicating that the growth defect in HMVECs cannot be overcome by infecting cells at higher multiplicities of infection. Similar results were obtained with the infectious recombinant viruses produced from the TRΔUS20 (clone 1.2) and TRUS20stop (clone 2.2) BACs (data not shown). The replication kinetics of the US20 revertant virus (TRUS20HA) in HMVECs was similar to that of TRwt (Fig. 5), thus indicating that the defective-growth phenotype of the US20-deficient viruses in endothelial cells was due to the specific inactivation of the US20 coding sequence.

pUS20 is required for efficient accumulation of E and L viral mRNAs and proteins in various types of endothelial cells. To gain further insight into the defective phenotype of US20-null viruses in endothelial cells, we first evaluated the kinetics of viral DNA synthesis by qPCR in HMVECs infected with the parental TRwt or the TRUS20stop viruses. Compared with TRwt, DNA replication of the US20-deficient virus in HMVECs was substantially absent over the entire replication cycle (Fig. 6A), thus indicating that inactivation of the *US20* gene caused a defect in virus replication in the endothelial cells that occurred prior to the onset of viral DNA synthesis.

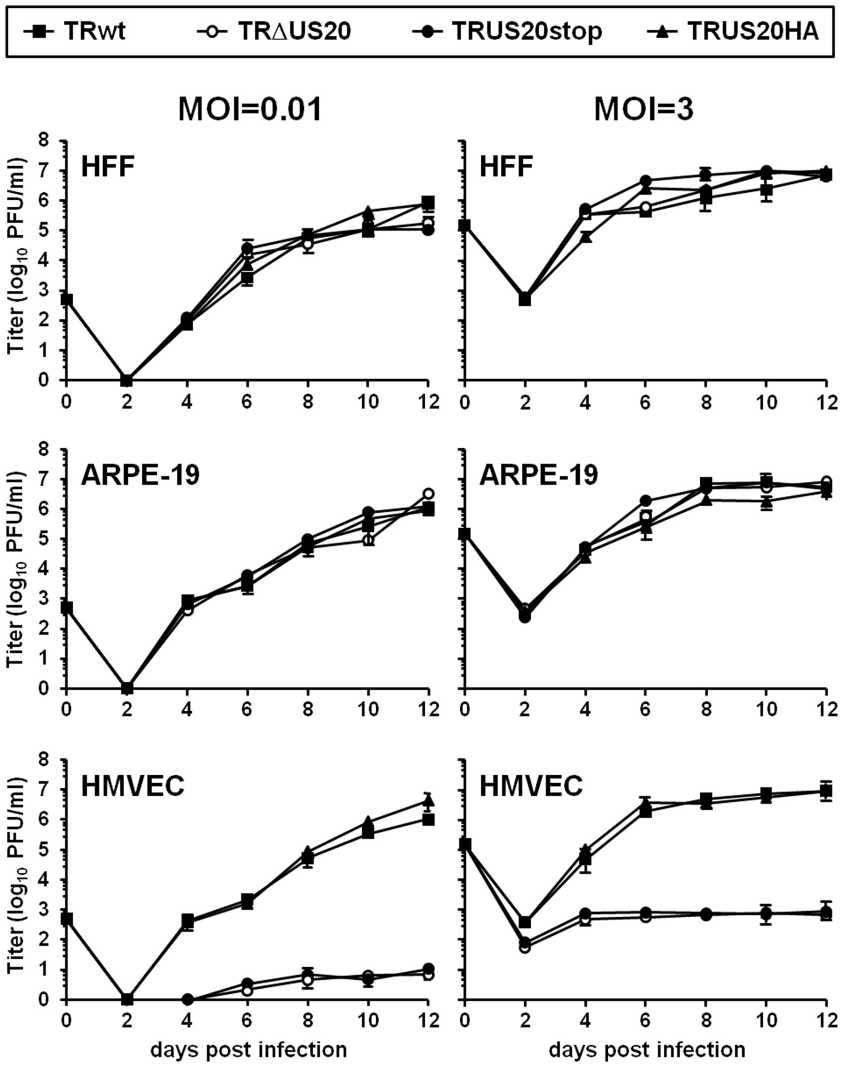

FIG 5 Growth kinetics of US20-deficient viruses in fibroblasts and epithelial and endothelial cells. HFFs, ARPE-19, and HMVECs were infected with TRwt, TRΔUS20 (clone 1.1), TRUS20stop (clone 2.1), or TRUS20HA at an MOI of 0.01 PFU/cell for multistep growth analysis or at an MOI of 3 PFU/cell for single-step growth analysis. The extent of virus replication at different times p.i. was then determined by titrating the infectivity of supernatants of cell suspensions on HFFs and quantifying IEAs by immunoperoxidase staining. The data shown are the averages of the results of two experiments ± SD.

To explore this observation further and to define better the phase of the HCMV replication cycle affected by the lack of pUS20, we evaluated the accumulation of representative IE, E, and L proteins. To this end, immunoblot assays were performed with cell extracts prepared at various times p.i. from HFFs and HMVECs that had been infected with TRwt or TRUS20stop. Expression levels of IEA (IE1 and IE2), UL44, and UL99 were measured as controls for IE, E, and L proteins, respectively (Fig. 6B). As expected, tested viral proteins accumulated with the same kinetics in HFFs infected with either TRwt or TRUS20stop. In contrast, in HMVECs infected with the US20 mutant virus, the expression of IEA was reduced by about 2-fold, as estimated by densitometric quantification, in comparison to that seen with TRwt, whereas that of UL44 and UL99 was substantially suppressed (Fig. 6B). Therefore, the absence of pUS20 in these cells prevented the normal progression of the viral replication cycle and caused a major defect prior to the expression of E proteins.

To test whether the lack of E and L protein expression in endothelial cells infected with the US20-null virus was due to an impairment of their RNA accumulation, mRNA was purified at various times p.i. from HMVECs that had been infected with either TRwt or TRUS20stop and was analyzed by real-time RT-PCR for IE1, UL44, and UL99 mRNA content. Figure 6C shows that, at all times analyzed, TRUS20stop failed to express a significant level of either UL44 or UL99 mRNA, whereas, according to the results obtained by the immunoblot analysis of viral protein expression (Fig. 6B), it produced reduced levels of IE1 mRNA. Thus, these results indicate that the defective-growth phenotype of US20-deficient viruses in endothelial cells arose from the lack of transcription of E and L genes.

Next, to rule out the possibility that the lack of E and L gene expression in endothelial cells was due to a defect restricted to HMVECs only, different types of endothelial cells able to support the productive replication of clinical isolates of HCMV (18, 20) were infected with TRwt, TRΔUS20, TRUS20stop, or TRUS20HA; viral titers and the frequency of IEA, E, and L expression were then

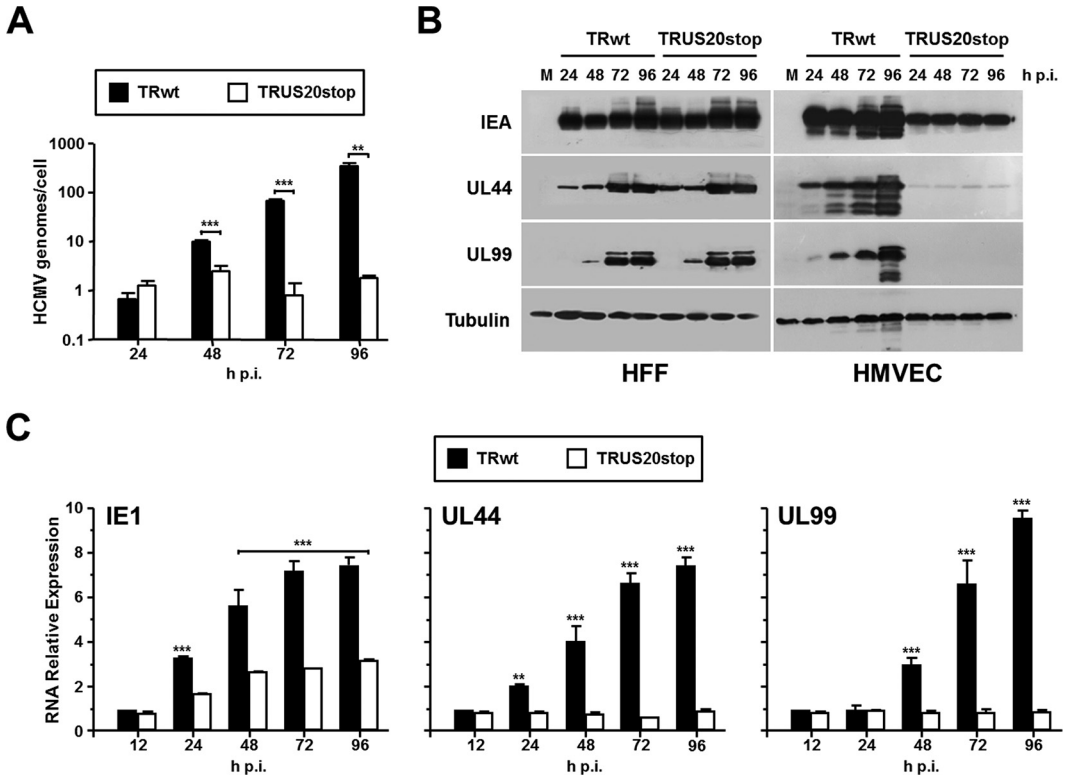

FIG 6 Replication of US20-deficient viruses in endothelial cells is blocked at a stage prior to the expression of E genes. (A) Lack of viral DNA synthesis in endothelial cells infected with a US20 mutant virus. HMVECs were infected with TRwt or TRUS20stop (MOI = 1 PFU/cell), and at the indicated times p.i., total genomic DNA was isolated to quantify viral DNA levels by qPCR. The data shown are the mean values of the results of two independent experiments ± SD. **, $P < 0.001$; ***, $P < 0.0001$ (compared to the amount of viral DNA measured in cells infected with TRwt). (B) Expression of representative IE, E, and L proteins in HFFs and HMVECs infected with TRwt or TRUS20stop viruses. HFFs and HMVECs were infected with TRwt or TRUS20stop (MOI = 1 PFU/cell). At the indicated times p.i., total protein cell extracts were prepared and analyzed by immunoblotting with anti-IEA, UL44, or UL99 MAbs. Tubulin immunodetection served as a control for equal protein loading. HMVECs panels were overexposed to detect the faint UL44 signal in extracts from TRUS20stop-infected cells. (C) The *US20* gene is required for E and L gene expression in endothelial cells. HMVECs were infected with TRwt or TRUS20stop (MOI = 1 PFU/cell). Total RNA was isolated at the indicated hours p.i. and reverse transcribed. Real-time RT-PCR was carried out with the appropriate IE1, UL44, UL99, and β-actin primers to quantify the expression levels of selected viral transcripts. For each time point, IE1, UL44, and UL99 mRNA amounts were normalized to the levels of the β-actin mRNA. For quantification analysis, values at each time point are relative to the value observed with cells infected with TRwt for 12 h (calibrator sample), which was set at 1. The results are shown as fold change of mRNA expression compared to the values of the calibrator sample and as the mean values of the results of two independent experiments ± SD of technical triplicates. **, $P < 0.001$; ***, $P < 0.0001$.

determined at various time intervals. As observed for HMVECs, inactivation of the US20 ORF severely reduced virus replication in both HUVECs and primary lymphatic endothelial cells (LECs) (Fig. 7A). Again, the growth defect was associated with the failure of US20-deficient viruses to express adequate amounts of E and L proteins (Fig. 7B), thus indicating that the defective phenotype does not depend on the origin of the endothelial cell.

Altogether, these results indicate a role for US20 protein in regulating the efficient progression of the viral replicative cycle, mostly beyond the IE phase, in different types of endothelial cells.

US20-null viruses are defective for a postentry event in endothelial cells. Next, we investigated whether the reduction of IE gene expression observed in endothelial cells infected with US20-deficient viruses could result from inefficient adsorption and/or entry of genotypically *US20*-negative virions. To evaluate the adsorption, HMVECs were infected with equivalent amounts of partially purified TRwt or TRUS20stop virions (normalized to equivalent genome copy numbers by qPCR) for 1 h at 4°C, thus allowing the attachment of virus particles only. The cells were then extensively washed, and total DNA was purified in order to measure the amount of viral DNA associated with cells by qPCR. As shown in Fig. 8A, the amounts of TRUS20stop DNA bound to HMVECs were not significantly different from those measured for TRwt, indicating the successful adsorption of both viruses to endothelial cells. The addition of trypsin before DNA isolation from samples of TRwt- or TRUS20stop-infected HMVECs severely reduced the amount of measurable HCMV DNA, thus confirming that the majority of the quantified DNA was present in viral particles bound to endothelial cells.

To test entry, HMVEC cell monolayers were infected with equal amounts of TRwt or TRUS20stop virions at 4°C for 1 h and then shifted to 37°C for different times to allow entry of viral particles bound to cell surfaces. Before DNA isolation, infected cells were treated with trypsin to remove virions bound to the cell surface but not yet internalized. Quantification of viral DNA by qPCR showed that the amounts of cell-associated viral DNA at 1, 2, and 4 h were similar for TRwt and TRUS20stop (Fig. 8B). This shows that the lack of the *US20* gene does not affect the ability of genotypically *US20*-negative HCMV virions to enter into endothelial cells and further sustains the view that US20 regulates

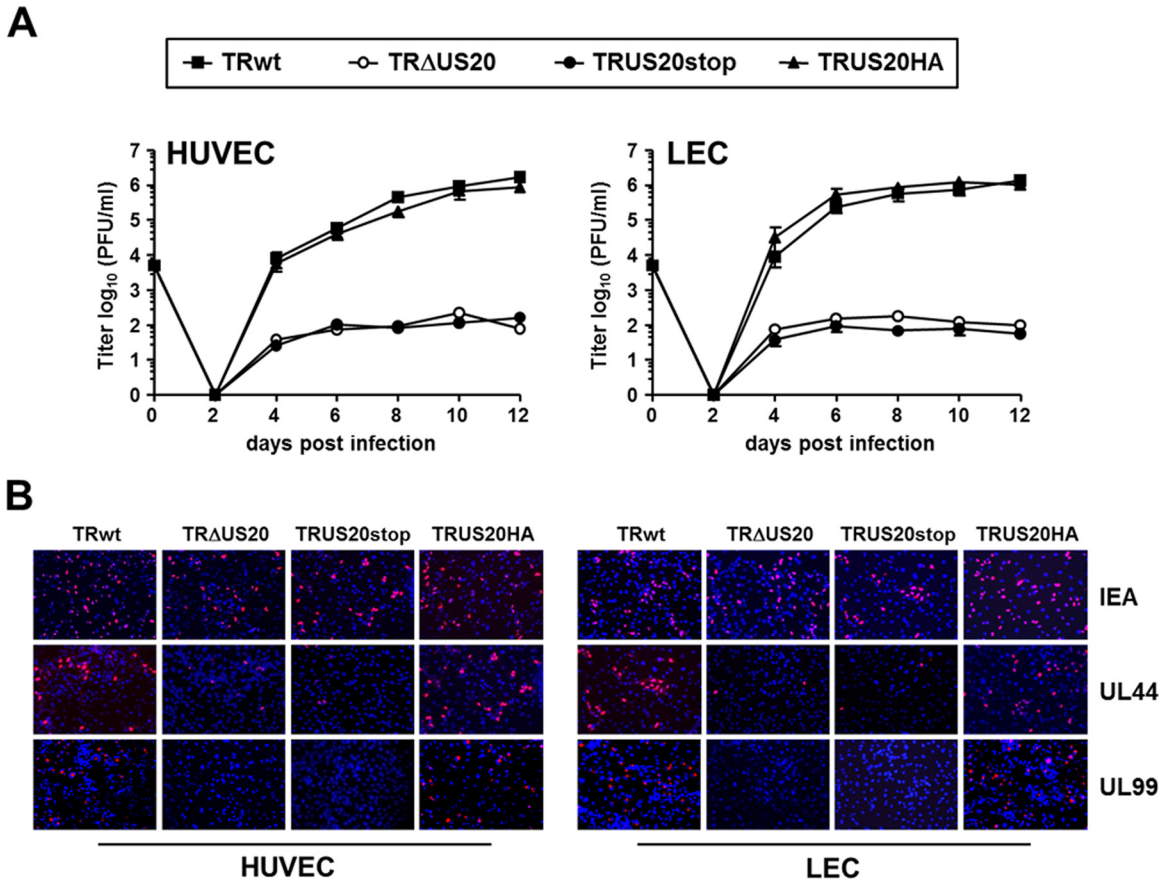

FIG 7 US20-deficient viruses fail to express E and L proteins in different types of endothelial cells. (A) US20-null viruses are defective for growth in HUVECs and LECs. HUVECs and LECs were infected with TRwt, TRΔUS20 (clone 1.1), TRUS20stop (clone 2.1), or TRUS20HA at an MOI of 0.1 PFU/cell. The extent of virus replication at different days p.i. was determined by titrating the infectivity of supernatants of cell suspensions on HFFs by anti-IEA staining. The data shown are the averages of the results of three independent experiments ± SD. (B) Lack of expression of E and L proteins in HUVECs and LECs infected with US20 mutant viruses. HUVECs and LECs were infected with TRwt, TRΔUS20 (clone 1.1), TRUS20stop (clone 2.1), or TRUS20HA at an MOI of 0.1 PFU/cell. At 24, 48, or 96 h p.i., cells were fixed, permeabilized, and immunostained with anti-IEA, UL44, or UL99 MAbs, respectively. Images of ECs infected with US20-null viruses for 48 and 96 h p.i. were purposely chosen to include positive cells to show virus addition, since random fields were in the majority negative for UL44 and UL99 staining. Data are representative of the results of three independent experiments.

postentry events involved in progression of the HCMV replication cycle in endothelial cells.

DISCUSSION

In this study, we characterized the expression profile of the *US20* gene product and provided evidence that the lack of the gene has a significant impact on the ability of HCMV to replicate in endothelial cells, thus suggesting an important role of this protein in HCMV dissemination, pathogenesis, and persistence in the host.

The *US20* gene of a clinical isolate of HCMV encodes a protein doublet expressed with early kinetics during the viral replicative cycle. This observation agrees with previous reports that demonstrated the accumulation of an early 2.85-kb tricistronic mRNA that spans the region initiating at the start of the US20 transcription initiation site and terminating at the polyadenylation signal downstream of US18 (7, 40, 41). Moreover, we showed that the pUS20 doublet occurs as a consequence of differential degrees of protein glycosylation, also sustained by the results of prediction analyses that identified a potential site of N-glycosylation at position 242 within the C-terminal tail of the US20 protein. Thus, among the US12 family members that have been characterized at the protein level to date (13, 14), pUS20 is the first to show a posttranslational modification through the addition of sugar moieties. Moreover, the complete EndoH sensitivity of the slower-migrating pUS20 band from infected cell extracts prepared at late times of infection (Fig. 2C) indicates that it contained immature, high-mannose N-linked oligosaccharides and that it had not reached the Golgi apparatus, to which most herpesvirus glycoproteins are transported and where their N-linked sugars processed to more-complex EndoH-resistant oligosaccharides (42). The idea of the localization and retention of pUS20 in the ER is sustained further by the results of the immunofluorescence analysis that showed an association with calreticulin-positive compartments throughout the virus cycle (Fig. 3D). Furthermore, the lack of any significant association of pUS20 with cellular and viral markers of the cVAC (Fig. 3C), in contrast with that previously observed for other US12 family members, such as US14, US16, US17, and US18 (13, 14), suggests that pUS20 is unlikely to be involved in the final maturation and egress of HCMV virions. Finally, we predicted the membrane topology of pUS20 using different algorithms; the results indicated a unique topology profile, consisting of seven TMDs. Indeed, experimental investigation confirmed this predic-

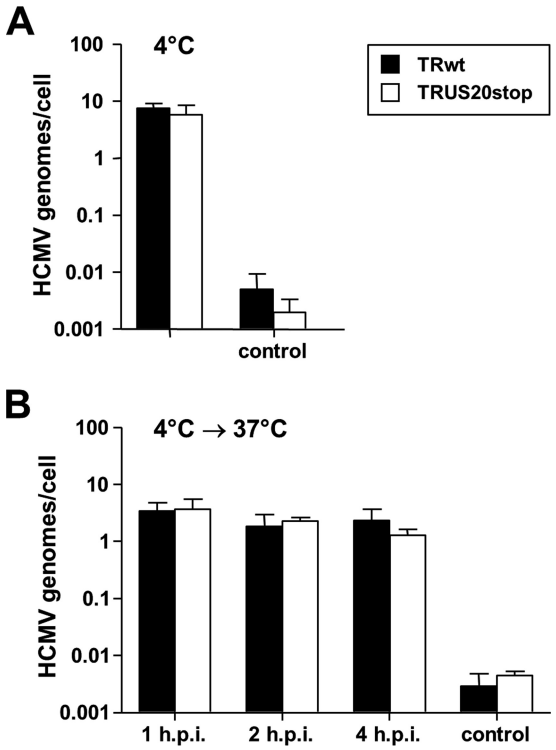

FIG 8 Attachment of a US20-deficient virus and entry of the virus into endothelial cells. (A) Adsorption of a US20-null virus to HMVECs. HMVECs were infected with equal numbers of TRwt or TRUS20stop virion particles at 4°C for 1 h to allow virus adsorption and then washed twice with PBS. To determine the extent of virus attachment, cell-associated viral DNA was then quantified by qPCR and normalized to the level of the 18S rRNA gene. Trypsin treatment of samples of infected HMVECs before DNA isolation was performed as a control to verify that the quantified DNA was from viral particles bound to cells (control bars). (B) Entry of a US20 mutant virus in endothelial cells. HMVECs were infected with equal numbers of TRwt or TRUS20stop virion particles at 4°C for 1 h, washed twice with PBS, and then shifted to 37°C for 1, 2, or 4 h to allow virus entry into the cells. Before DNA isolation, at each time point, infected HMVECs were treated with trypsin to remove virions bound to cell surfaces but not internalized. To ensure the efficiency of the trypsin treatment in removing bound virus, control cultures were treated immediately after adsorption at 4°C, replated, and returned to 37°C for 5 h before DNA isolation (control bars). Cell-associated HCMV DNA was then quantified by qPCR and normalized to the level of the 18S rRNA gene. The data shown represent the averages of the results of three independent experiments ± SD.

tion (Fig. 4), placing the N terminus of pUS20 on the cytosol side of a membrane, for example, that of an ER-derived compartment, and its C terminus on the luminal side. In this regard, a previous *in silico* analysis of US12 family members suggested opposite membrane orientations by analogy to G-protein-coupled receptors (GPCRs) (11). In that study, however, a phylogenetic analysis of US12 proteins in comparison to previously characterized viral and cellular GPCRs and other 7TMD proteins indicated that US12 proteins represent a distinct branch of the 7TMD superfamily (11). Thus, it is likely that the limited level of similarity to GPCRs (11) explains the different membrane orientation observed for pUS20. Moreover, in a preliminary bioinformatics analysis, we observed that the US20 ORF shares about 20% amino acid identity with the Golgi antiapoptotic-associated protein (GAAP), a member of the predicted transmembrane BAX inhibitor-1 motif (TMBIM)-containing protein family. TMBIM proteins are a group of at least six highly conserved cell death regulators expressed in mammals and with homologs in fish, insects, plants, yeasts, and viruses (43). In particular, viral counterparts of human GAAP (hGAAP) have been identified in some strains of vaccinia virus (VACV) and camelpox virus (CMLV) and have been shown to inhibit apoptosis induced by both intrinsic and extrinsic proapoptotic stimuli (25, 44). A detailed experimental mapping of the transmembrane topology of hGAAP and viral GAAP (vGAAP), as well as of BAX inhibitor 1 (BI-1), revealed a cytosolic orientation of their N termini, as we observed for pUS20, and a six-TMD topology with a putative reentrant loop at the C terminus, thus placing the C terminus of these TMBIM proteins on the cytosolic side of a membrane (25). However, it is worth noting that our bioinformatics analysis highlighted that the last predicted transmembrane domain of GAAP and BI-1 is less hydrophobic than that of pUS20. Thus, this variance may account for the different membrane topology of the C terminus of pUS20 in comparison to those of the GAAP and BI-1 proteins.

It is therefore likely that the topology profile of pUS20 may have important implications regarding its interactions with other cellular and/or viral proteins and, therefore, its functions.

Indeed, we observed that genotypically *US20*-negative virions selectively failed to replicate specifically in different types of endothelial cells, whereas they grew normally in both fibroblasts and epithelial cells. The growth defect of US20-null viruses in endothelial cells was associated with an impairment of the capacity of the viral replication cycle to progress beyond the entry and IE phases. The endothelium-specific growth defect was observed using different US20 mutant viruses (two RVTRΔUS20 virus strains from two independent clones and two US20stop mutants, generated by the insertion of a stop codon at its N terminus). This observation indicates that the inability of US20-null viruses to replicate in endothelial cells was likely due to the mutations made to the US20 locus and not to potential second-site mutations that could have affected neighboring or more-distant genes. The specificity of the US20-dependent growth defect was then further confirmed via restoration of the wild-type-level growth rate in endothelial cells infected with the revertant virus TRUS20HA, in which the US20 deletion was repaired by inserting the US20 ORF sequence back into the TRΔUS20 genome fused in frame with a C-terminal HA tag.

The lack of a significant effect on entry into endothelial cells suggests that pUS20 contributes to the HCMV tropism in this cell type through a pathway that is distinct from that relevant to US16 (14). For the latter, in fact, we observed a requirement for IE gene expression and delivery of the viral genome to the nucleus in both endothelial and epithelial cells (14). The inability of US16-deficient virions to express IE genes in these cell types has since been related to a specific entry defect caused by the lack of adequate amounts of the gH/gL/UL128–UL131 envelope pentameric complex, which mediates HCMV entry into endothelial and epithelial cells (Luganini and Gribaudo, unpublished). Thus, it is likely that pUS16 regulates HCMV cell tropism through a pathway that develops in producer cells and in which pUS16 acts as a tropism factor by dictating a critical stage in the late maturation of HCMV related to the final assembly of endothelio- and epitheliotropic progeny. Here, we observed that the replication of US20-null viruses in epithelial cells was not significantly different from that observed in fibroblasts (Fig. 5); it is therefore unlikely that US20 influences the abundance of the virion pentameric complex, as

observed for US16-null viruses. However, an effect of pUS20 on virion composition cannot be excluded, since we measured a reduced level of IE gene expression in endothelial cells infected with a US20-deficient virus, which may indicate a lack of an adequate content of tegument proteins, such as pUL82 (pp71) and pUL83 (pp65), known to be important for efficient IE gene expression in the newly infected cell (45, 46). Further proteomics analysis of purified US20-null virion particles may thus help to define their content and elucidate the relationship between virion composition and the reduced level of IE protein expression observed in infected endothelial cells.

Since it has been reported that the murine M45 gene mediates murine cytomegalovirus (MCMV) replication in endothelial cells by inhibiting apoptosis (47) and given the predicted similarity of pUS20 to hGAAP and vGAAP (obtained by bioinformatics), we hypothesized that the failure of US20 mutant viruses to replicate in endothelial cells might stem from their inability to counteract the apoptotic antiviral response in infected cells. However, preliminary analyses did not reveal any significant differences in the death rate of HMVECs infected with a US20-null virus compared to cells infected with the parental TR virus, nor was any significant variation in caspase-3 activity observed between cell extracts prepared from TRUS20stop- or TRwt-infected HMVECs and stimulated with a strong proapoptotic stimulus, such as doxorubicin (data not shown). Thus, pUS20 does not seem to play a significant role in regulating apoptosis despite its similarity to members of the TMBIM family. However, the lack of any apparent antiapoptotic activity of pUS20 may be explained by the absence of the typical cluster of charged residues found in the C terminus of hGAAP, vGAAP, and BI-1 proteins and required to counteract cell apoptosis in response to both intrinsic and extrinsic stimuli (43, 44). Thus, the growth defect of US20-null viruses in endothelial cells cannot be ascribed to a lack of an adequate viral antiapoptotic activity, as previously observed for M45-deficient viruses (47).

During coevolution with its host, HCMV has developed the capacity to replicate in a wide range of cell types by exploiting different combinations of cell receptors, entry pathways, envelope glycoprotein complexes, and requirements for postentry viral tropism factors. So far, however, little is known about the functions exerted by viral tropism factors that act at a postentry stage and regulate, in a cell type-specific manner, subsequent stages of the virus replication cycle. In addition to the HCMV US20 and MCMV M45 (47) proteins, two other HCMV proteins were recently reported to contribute to HCMV tropism in endothelial cells by regulating post-immediate-early phases in the viral replication cycle (48, 49, 50). In these studies, the UL135 and UL136 proteins encoded within the UL133-to-UL138 locus of a clinical strain of the virus (48) were found to be required for efficient HCMV replication in primary endothelial cells (50). The genes encoding those proteins were demonstrated to be dispensable for virus entry and normal expression of representative IE, E, and L proteins (49, 50). However, the failure of UL135- and UL136-deficient viruses to produce infectious progeny in infected endothelial cells was related to defects in different stages of the final maturation of the virion, such as formation of the cVAC, the secondary envelopment, and egress (50). It was thus concluded that UL135 and UL136 function as determinants of viral tropism for endothelial cells by regulating the proper host membrane trafficking pathway required for an efficient viral maturation process in this specific cell type (50). Thus, UL135 and UL136 seem to act at stages of the HCMV replication cycle downstream from that primarily affected by the lack of functional pUS20. In fact, in endothelial cells infected with a US20 mutant virus, we observed a severe defect in the progression of the viral gene expression cascade, mostly after the IE phase, and a failure in viral DNA replication (Fig. 6), both of which indicate a requirement of pUS20 for efficient expression of E genes. Future studies will be required to verify the involvement, if any, of pUS20 in promoting efficient viral E gene expression in infected endothelial cells.

The requirement for the HCMV tropism in endothelial cells, however, is not the sole function that can be assigned to US20. In fact, it was recently reported that the *US20* gene, in concert with *US18*, reduces the cell surface expression of MICA by promoting its lysosomal degradation (16). Nevertheless, no clear association of pUS18 and pUS20 with lysosomes was observed in US18- or US20-expressing U373 cells or in HCMV-infected HFFs (16). Thus, pUS20 may represent a further example of a multifunctional HCMV protein that regulates different features of the viral replication cycle and virus-host interactions.

Although future investigations are required to define in more detail the mechanism by which the US20 protein regulates the tropism for endothelial cells, the results of the present study sustain the view that the members of the *US12* gene family encode a series of regulatory proteins involved in a variety of different intracellular regulatory networks within HCMV-infected cells. In fact, inactivation of different members may affect the normal virion composition (15) and the virus's ability to modulate the host immune response (16) or, as we reported for US16 and US20, may impact viral replication in specific cell types. Our current knowledge about the functions of pUS12 proteins is therefore coherent with the hypothesis that individual *US12* gene family members have evolved the ability to fulfill different and specific functions by adapting a host-derived common and flexible structural protein scaffold, one that is intimately associated with various cellular membranes, to new purposes (11, 51). In this model, changes in the highly divergent N- and C-terminal amino acid sequences in the different *US12* ORFs (11) may permit specific interactions with other cellular and/or viral proteins to occur that may regulate a broad range of specific activities within infected cells.

ACKNOWLEDGMENTS

We gratefully thank Jay Nelson (VGTI, Oregon Health Science University) for providing the TR BAC, Tom Shenk (Princeton University) for the pCGN71, Neal Copeland (NCI, Frederick, MD) for the *E. coli* SW102 strain, Dong Yu (Washington University) for pGalK-Kan, Arnaldo Caruso (University of Brescia) for lymphatic endothelial cells, and Andrea Gallina (University of Milan) for ARPE-19 cells.

This work was supported by grants from the Italian Ministry for Universities and Scientific Research (Research Programs of Significant National Interest, PRIN 2010-11, grant no. 2010PHT9NF) to G.G. and Ex-60% from the University of Turin to A.L. and G.G.

REFERENCES

1. **Britt W.** 2008. Manifestations of human cytomegalovirus infection: proposed mechanisms of acute and chronic disease. Curr Top Microbiol Immunol **325:**417–470.
2. **Landolfo S, Gariglio M, Gribaudo G, Lembo D.** 2003. The human cytomegalovirus. Pharmacol Ther **98:**269–297. http://dx.doi.org/10.1016/S0163-7258(03)00034-2.
3. **Mocarski ES, Shenk T, Griffiths PD, Pass RF.** 2013. Cytomegaloviruses, p 1960–2014. *In* Knipe DM, Howley PM, Cohen JI, Griffin DE, Lamb RA, Martin MA, Racaniello VR, Roizman B (ed), Fields virology, 6th ed. Lippincott Williams & Wilkins, Philadelphia, PA.

4. **Goodrum F, Caviness K, Zagallo P.** 2012. Human cytomegalovirus persistence. Cell Microbiol **14:**644–655. http://dx.doi.org/10.1111/j.1462-5822.2012.01774.x.
5. **Murphy E, Shenk T.** 2008. Human cytomegalovirus genomes. Curr Top Microbiol Immunol **325:**1–20.
6. **Davison AJ, Holton M, Dolan A, Dargan DJ, Gathered D, Hayward GS.** 2013. Comparative genomics of primate cytomegaloviruses, p 1–22. *In* Reddehase MJ (ed), Cytomegaloviruses: from molecular pathogenesis to intervention, vol 1. Caister Academic Press, London, United Kingdom.
7. **Stern-Ginossar N, Weisburd B, Michalski A, Le VT, Hein MY, Huang SX, Ma M, Shen B, Qian SB, Hengel H, Mann M, Ingolia NT, Weissman JS.** 2012. Decoding human cytomegalovirus. Science **338:**1088–1093. http://dx.doi.org/10.1126/science.1227919.
8. **Van Damme E, Van Loock M.** 2014. Functional annotation of human cytomegalovirus gene products: an update. Front Microbiol **5:**218. http://dx.doi.org/10.3389/fmicb.2014.00218.
9. **Dunn W, Chou C, Li H, Hai R, Patterson D, Stolc V, Zhu H, Liu F.** 2003. Functional profiling of a human cytomegalovirus genome. Proc Natl Acad Sci U S A **100:**14223–14228. http://dx.doi.org/10.1073/pnas.2334032100.
10. **Yu D, Silva MC, Shenk T.** 2003. Functional map of human cytomegalovirus AD169 defined by global mutational analysis. Proc Natl Acad Sci U S A **100:**12396–12401. http://dx.doi.org/10.1073/pnas.1635160100.
11. **Lesniewski M, Das S, Skomorovska-Prokvolit Y, Wang FZ, Pellet PE.** 2006. Primate cytomegalovirus US12 gene family: a distinct and diverse clade of seven-transmembrane proteins. Virology **354:**286–298. http://dx.doi.org/10.1016/j.virol.2006.06.035.
12. **Murphy E, Yu D, Grimwood J, Schmutz J, Dickson M, Jarvis MA, Hahn G, Nelson JA, Myers RM, Shenk T.** 2003. Coding potential of laboratory and clinical strains of human cytomegalovirus. Proc Natl Acad Sci U S A **100:**14976–14981. http://dx.doi.org/10.1073/pnas.2136652100.
13. **Das S, Pellet PE.** 2007. Members of the HCMV US12 family of predicted heptaspanning membrane proteins have unique intracellular distributions, including association with the cytoplasmic virion assembly complex. Virology **361:**263–273. http://dx.doi.org/10.1016/j.virol.2006.11.019.
14. **Bronzini M, Luganini A, Dell'Oste V, De Andrea M, Landolfo S, Gribaudo G.** 2012. The US16 gene of human cytomegalovirus is required for efficient viral infection of endothelial and epithelial cells. J Virol **86:**6875–6888. http://dx.doi.org/10.1128/JVI.06310-11.
15. **Gurczynski S, Das S, Pellet PE.** 2014. Deletion of the human cytomegalovirus US17 gene increases the ratio of genomes per infectious unit and alters regulation of immune and endoplasmic reticulum stress response genes at early and late times after infection. J Virol **88:**2168–2182. http://dx.doi.org/10.1128/JVI.02704-13.
16. **Fielding CA, Aicheler R, Stanton RJ, Wang ECY, Han S, Seirafian S, Davies J, McSharry BP, Weekes MP, Antrobus PR, Prod'homme V, Blanchet FP, Sugrue D, Cuff S, Roberts D, Davison AJ, Lehner PJ, Wilkinson GWG, Tomasec P.** 2014. Two novel human cytomegalovirus NK cell evasion functions target MICA for lysosomal degradation. PLoS Pathog **10:**e1004058. http://dx.doi.org/10.1371/journal.ppat.1004058.
17. **Hai R, Chu A, Li H, Unamoto S, Rider P, Liu F.** 2006. Infection of human cytomegalovirus in cultured human gingival tissue. Virol J **3:**84. http://dx.doi.org/10.1186/1743-422X-3-84.
18. **Fiorentini S, Luganini A, Dell'Oste V, Lorusso B, Cervi E, Caccuri F, Bonardelli S, Landolfo S, Caruso A, Gribaudo G.** 2011. Human cytomegalovirus productively infects lymphatic endothelial cells and induces a secretome that promotes angiogenesis and lymphangiogenesis through interleukin-6 and granulocyte macrophage colony-stimulating factor. J Gen Virol **92:**650–660. http://dx.doi.org/10.1099/vir.0.025395-0.
19. **Smith IL, Taskintuna I, Rahhal FM, Powell HC, Ai E, Mueller AJ, Spector SA, Freeman WR.** 1998. Clinical failure of CMV retinitis with intravitreal cidofovir is associated with antiviral resistance. Arch Ophthalmol **116:**178–185.
20. **Ryckman BJ, Jarvis MA, Drummond DD, Nelson JA, Johnson DC.** 2006. Human cytomegalovirus entry into epithelial and endothelial cells depends on genes UL128 to UL150 and occurs by endocytosis and low-pH fusion. J Virol **80:**710–722. http://dx.doi.org/10.1128/JVI.80.2.710-722.2006.
21. **Warming S, Costantino N, Court DL, Jenkins NA, Copeland NG.** 2005. Simple and highly efficient BAC recombineering using galK selection. Nucleic Acids Res **33:**e36. http://dx.doi.org/10.1093/nar/gni035.
22. **Brune W, Nevels M, Shenk T.** 2003. Murine cytomegalovirus m41 open reading frame encodes a Golgi-localized antiapoptotic protein. J Virol **77:**11633–11643. http://dx.doi.org/10.1128/JVI.77.21.11633-11643.2003.
23. **Luganini A, Caposio P, Landolfo S, Gribaudo G.** 2008. Phosphorothioate-modified oligodeoxynucleotides inhibit human cytomegalovirus replication by blocking virus entry. Antimicrob Agents Chemother **52:**1111–1120. http://dx.doi.org/10.1128/AAC.00987-07.
24. **Das S, Pellet PE.** 2011. Spatial relationships between markers for secretory and endosomal machinery in human cytomegalovirus-infected cells versus those in uninfected cells. J Virol **85:**5864–5879. http://dx.doi.org/10.1128/JVI.00155-11.
25. **Carrara G, Saraiva N, Gubser C, Johnson BF, Smith GL.** 2012. Six-transmembrane topology for Golgi anti-apoptotic protein (GAAP) and Bax inhibitor 1 (BI-1) provides model for the transmembrane Bax inhibitor-containing motif (TMBIM) family. J Biol Chem **287:**15896–15905. http://dx.doi.org/10.1074/jbc.M111.336149.
26. **O'Connor CM, Shenk T.** 2012. Human cytomegalovirus pUL78 G protein-coupled receptor homologue is required for timely cell entry in epithelial cells but not fibroblasts. J Virol **86:**11425–11433. http://dx.doi.org/10.1128/JVI.05900-11.
27. **Caposio P, Luganini A, Hahn G, Landolfo S, Gribaudo G.** 2007. Activation of the virus-induced IKK/NF-κB signalling axis is critical for the replication of human cytomegalovirus in quiescent cells. Cell Microbiol **9:**2040–2054. http://dx.doi.org/10.1111/j.1462-5822.2007.00936.x.
28. **Tanaka N, Kimura H, Iida K, Saito K, Tsuge I, Yoshimi A, Matsuyama T, Morishima T.** 2000. Quantitative analysis of cytomegalovirus load using a real-time PCR assay. J Med Virol **60:**455–462. http://dx.doi.org/10.1002/(SICI)1096-9071(200004)60:4<455::AID-JMV14>3.0.CO;2-Q.
29. **Gribaudo G, Riera L, Rudge TL, Caposio P, Johnson LF, Landolfo S.** 2002. Human cytomegalovirus infection induces cellular thymidylate synthase gene expression in quiescent fibroblasts. J Gen Virol **83:**2983–2993.
30. **Das S, Skomorovska-Prokvolit Y, Wang FZ, Pellet PE.** 2006. Infection-dependent nuclear localization of US17, a member of the US12 family of human cytomegalovirus-encoded seven-transmembrane proteins. J Virol **80:**1191–1203. http://dx.doi.org/10.1128/JVI.80.3.1191-1203.2006.
31. **Das S, Vasanji A, Pellet PE.** 2007. Three-dimensional structure of the human cytomegalovirus virion assembly complex includes a reoriented secretory apparatus. J Virol **81:**11861–11869. http://dx.doi.org/10.1128/JVI.01077-07.
32. **Tandon R, Mocarski ES.** 2012. Viral and host control of cytomegalovirus maturation. Trends Microbiol **20:**392–401. http://dx.doi.org/10.1016/j.tim.2012.04.008.
33. **Hirokawa T, Boon-Chieng S, Mitaku S.** 1998. SOSUI: classification and secondary structure prediction system for membrane proteins. Bioinformatics **14:**378–379. http://dx.doi.org/10.1093/bioinformatics/14.4.378.
34. **Claros MG, von Heijne G.** 1994. TopPred II: an improved software for membrane protein structure predictions. Comput Appl Biosci **10:**685–686.
35. **Krogh A, Larsson B, von Heijne G, Sonnhammer EL.** 2001. Predicting transmembrane protein topology with a hidden Markov model: application to complete genomes. J Mol Biol **305:**567–580. http://dx.doi.org/10.1006/jmbi.2000.4315.
36. **Nugent T, Jones D.** 2009. Transmembrane protein topology prediction using support vector machines. BMC Bioinformatics **10:**159. http://dx.doi.org/10.1186/1471-2105-10-159.
37. **Nakamura N, Rabouille C, Watson R, Nilsson T, Hui N, Slusarewicz P, Kreis TE, Warren G.** 1995. Characterization of a cis-Golgi matrix protein, GM130. J Cell Biol **131:**1715–1726. http://dx.doi.org/10.1083/jcb.131.6.1715.
38. **Bedard K, Szabo E, Michalak M, Opas M.** 2005. Cellular functions of endoplasmic reticulum chaperones calreticulin, calnexin, and ERp57. Int Rev Cytol **245:**91–121. http://dx.doi.org/10.1016/S0074-7696(05)45004-4.
39. **Adler B, Sinzger C.** 2013. Cytomegalovirus interstrain variance in cell type tropism, p 297–321. *In* Reddehase MJ (ed), Cytomegaloviruses: from molecular pathogenesis to intervention, vol 1. Caister Academic Press, London, United Kingdom.
40. **Guo YW, Huang ES.** 1993. Characterization of structurally tricistronic gene of human cytomegalovirus composed of U(s)18, U(s)19, and U(s)20. J Virol **67:**2043–2054.
41. **Towler JC, Ebrahimi B, Lane B, Davison AJ, Dargan DJ.** 2012. Human cytomegalovirus transcriptome activity differs during replication in human fibroblast, epithelial and astrocyte cell lines. J Gen Virol **93:**1046–1058. http://dx.doi.org/10.1099/vir.0.038083-0.
42. **Johnson DC, Spear PG.** 1983. O-linked oligosaccharides are acquired by

herpes simplex virus glycoproteins in the Golgi apparatus. Cell **32:**987–997. http://dx.doi.org/10.1016/0092-8674(83)90083-1.

43. **Rojas-Rivera D, Hetz C.** 2015. TMBIM protein family: ancestral regulators of cell death. Oncogene **34:**269–280. http://dx.doi.org/10.1038/onc.2014.6.
44. **Gubser C, Bergamaschi D, Hollinshead M, Lu X, van Kuppeveld FJ, Smith GL.** 2007. A new inhibitor of apoptosis from vaccinia virus and eukaryotes. PLoS Pathog **3:**e17. http://dx.doi.org/10.1371/journal.ppat.0030017.
45. **Penkert RR, Kalejta RF.** 2012. Tale of a tegument transactivator: the past, present and future of human CMV pp71. Future Virol **7:**855–869. http://dx.doi.org/10.2217/fvl.12.86.
46. **Cristea IM, Moorman NJ, Terhune SS, Cuevas CD, O'Keefe ES, Rout MP, Chait BT, Shenk T.** 2010. Human cytomegalovirus pUL83 stimulates activity of the viral immediate-early promoter through its interaction with the cellular IF16 protein. J Virol **84:**7803–7814. http://dx.doi.org/10.1128/JVI.00139-10.
47. **Brune W, Menard C, Heeseman J, Koszinowski UH.** 2001. A ribonucleotide reductase homolog of cytomegalovirus and endothelial cell tropism. Science **291:**303–305. http://dx.doi.org/10.1126/science.291.5502.303.
48. **Umashankar M, Petrucelli A, Cicchini L, Caposio P, Kreklywich CN, Rak M, Bughio F, Goldman DC, Hamlin KL, Nelson JA, Fleming WH, Streblow DN, Goodrum F.** 2011. A novel human cytomegalovirus locus modulates cell type-specific outcomes of infection. PLoS Pathog **7:**e1002444. http://dx.doi.org/10.1371/journal.ppat.1002444.
49. **Bughio F, Elliott DA, Goodrum F.** 2013. An endothelial cell-specific requirement for the UL133-UL138 locus of human cytomegalovirus for efficient virus maturation. J Virol **87:**3062–3075. http://dx.doi.org/10.1128/JVI.02510-12.
50. **Bughio F, Umashankar M, Wilson J, Goodrum F.** 2015. Human cytomegalovirus UL135 and UL136 genes are required for post-entry tropism in endothelial cells. J Virol http://dx.doi.org/10.1128/JVI.00284-15.
51. **Pellet PE, Roizman B.** 2013. Herpesviruses, p 1802–1822. *In* Knipe DM, Howley PM, Cohen JI, Griffin DE, Lamb RA, Martin MA, Racaniello VR, Roizman B (ed), Fields virology, 6th ed. Lippincott Williams & Wilkins, Philadelphia, PA.